

P_NFE Component of the UNIC Code

M. A. Smith, G. Palmiotti, C. Rabiti
Nuclear Engineering Division

D. Kaushik, A. Siegel, B. Smith
Mathematics and Computer Science Division

Argonne National Laboratory
9700 South Cass Avenue
Argonne, Illinois 60439

E. E. Lewis
Northwestern University
Department of Mechanical Engineering
Evanston, Illinois 6020

Email contact: masmith@anl.gov

ABSTRACT

A code package called UNIC is currently under development at Argonne (Argonne National Laboratory). This new code package is focused on high fidelity solutions for nuclear reactor plant operations. The focus of this paper is the development of a spherical harmonics method used to solve the neutron transport equation. This new code, called P_NFE, is just one of the components of UNIC. P_NFE is targeted for use on massively parallel platforms using the PETSc library developed at ANL. In this paper, an overview of the theory behind the spherical harmonics method is given along with some results obtained with a parallel implementation of the code.

Key Words: neutronics, spherical harmonics, finite element, unstructured mesh

1. INTRODUCTION

Recent work at Argonne has been focused on the development of a new high-fidelity system of software tools that model the overall nuclear plant behavior.¹ Within this framework, this paper focuses on a specific method implemented to solve the neutron transport equation. At present, there are several notable methods used in reactor analysis and other more general transport applications (shielding, deep well logging).² The most commonly known ones include: diffusion based nodal methods, discrete ordinates structured and unstructured methods, finite element based spherical harmonics, combinatorial geometry based collision probability and characteristics. There exists substantial experience with all of these methods in the nuclear industry and thus each individual method has well known advantages and disadvantages when compared with the other methods. As a consequence, these methods have been implemented

such that they are best utilized for specific problems found in the nuclear industry (discrete ordinates for shielding, nodal methods for reactor physics analysis, etc...).

One of the most well used methods currently employed for reactor analysis is the diffusion approximation. This approximation is typically employed at the whole-core level using assembly level homogenized cross sections in a nodal framework. To reproduce this capability, i.e. be able to rapidly solve problems based upon homogenized assemblies, we have focused the initial development in UNIC on a second-order spherical harmonics method. The spherical harmonics method² implements a continuous set of orthogonal functions to approximate the angular variable in the neutron transport equation and is generally well known in the nuclear industry. It is typically posed in either a finite element or finite difference spatial approximation, where both formulations lead to a large coupled system of equations for the angular approximation. The methods foremost weakness is that any transport problem which has discontinuities in the angular flux can require a high number of spherical harmonics. As the angular order increases to meet the discontinuity, the method becomes numerical inferior to other methodologies such as discrete ordinates or discontinuous angular finite elements. However, its use for solving homogenous problems without concern for ray effects has proven quite useful for reactor analysis. Since solving explicit full core geometries with acceptable space, angle, and energy resolution is computationally expensive, we can expect that some form of homogenization will still be required in the near term and thus the spherical harmonics methodology is quite useful. In general, however, we desire the ability to handle a wide variety of reactor problems and thus development of a general second-order solver appears to be a good complementary capability to the first-order methods currently under study in the UNIC framework.

2. SPHERICAL HARMONIC METHOD

The neutron transport methods for this work with the steady state first-order, multi-group equation²

$$\hat{\Omega} \cdot \bar{\nabla} \psi_g(\vec{r}, \hat{\Omega}) + \Sigma_{t,g}(\vec{r}) \psi_g(\vec{r}, \hat{\Omega}) = \sum_{g'=1}^G \int \Sigma_{s,g' \rightarrow g}(\vec{r}, \hat{\Omega} \cdot \hat{\Omega}') \psi_{g'}(\vec{r}, \hat{\Omega}') d\hat{\Omega}' + S_g(\vec{r}, \hat{\Omega}). \quad (1)$$

$\psi_g(\vec{r}, \hat{\Omega})$ represents the neutron angular flux and is a function of three space variables (x, y, z in \vec{r}) and two angular variables (θ and ϕ in $\hat{\Omega}$). The total cross section, $\Sigma_{t,g}(\vec{r})$, represents the sum of all possible neutron reaction probabilities at the point \vec{r} . Similarly, the scattering kernel $\Sigma_{s,g' \rightarrow g}(\vec{r}, \hat{\Omega}' \rightarrow \hat{\Omega}) d\hat{\Omega}$ represents the probability that a particle at \vec{r} traveling in the direction $\hat{\Omega}'$ is scattered into the direction $d\hat{\Omega}$ about $\hat{\Omega}$. Finally, $S_g(\vec{r}, \hat{\Omega})$ is a generic neutron source that includes fission sources as well as volumetric and boundary fixed sources. This equation can be simplified by merging all but the within group scattering ($g = g'$) into the group source to obtain the within group form of the transport equation

$$\begin{aligned} \hat{\Omega} \cdot \bar{\nabla} \psi_g(\vec{r}, \hat{\Omega}) + \Sigma_{t,g}(\vec{r}) \psi_g(\vec{r}, \hat{\Omega}) &= W_g(\vec{r}, \hat{\Omega}) + S_g(\vec{r}, \hat{\Omega}) \\ W_g(\vec{r}, \hat{\Omega}) &= \int \Sigma_{s,g \rightarrow g}(\vec{r}, \hat{\Omega} \cdot \hat{\Omega}') \psi_g(\vec{r}, \hat{\Omega}') d\hat{\Omega}'. \end{aligned} \quad (2)$$

2.1. Even Parity Transformation

Next, we transform this equation into an even parity form which is standard approach for second-order methods. First, the angular flux is split into even and odd parity components given by

$$\psi_g(\vec{r}, \hat{\Omega}) = \psi_g^+(\vec{r}, \hat{\Omega}) + \psi_g^-(\vec{r}, \hat{\Omega}), \quad (3)$$

where + denotes even parity and – denotes odd parity. The even and odd parity components of the flux have the following properties,

$$\begin{array}{cc} \text{Even} & \text{Odd} \\ \psi_g^+(\vec{r}, \hat{\Omega}) = \psi_g^+(\vec{r}, -\hat{\Omega}) & \psi_g^-(\vec{r}, \hat{\Omega}) = -\psi_g^-(\vec{r}, -\hat{\Omega}) \\ \int \psi_g^+(\vec{r}, \hat{\Omega}) d\Omega = \phi_g(\vec{r}) & \int \psi_g^-(\vec{r}, \hat{\Omega}) d\Omega = 0 \end{array} \quad (4)$$

where the function $\phi_g(\vec{r})$ represents the group scalar flux. Inserting Eq. (4) into Eq. (2) yields

$$\hat{\Omega} \cdot \vec{\nabla} [\psi_g^+(\vec{r}, \hat{\Omega}) + \psi_g^-(\vec{r}, \hat{\Omega})] + \Sigma_{t,g}(\vec{r}) [\psi_g^+(\vec{r}, \hat{\Omega}) + \psi_g^-(\vec{r}, \hat{\Omega})] = W_g(\vec{r}, \hat{\Omega}) + S_g(\vec{r}, \hat{\Omega}). \quad (5)$$

This equation leads to the first-order even and odd parity transport equations:

$$\text{Even Parity} \quad \hat{\Omega} \cdot \vec{\nabla} \psi_g^-(\vec{r}, \hat{\Omega}) + \Sigma_{t,g}(\vec{r}) \psi_g^+(\vec{r}, \hat{\Omega}) = W_g^+(\vec{r}, \hat{\Omega}) + S_g^+(\vec{r}, \hat{\Omega}) \quad (6)$$

$$\text{Odd Parity} \quad \hat{\Omega} \cdot \vec{\nabla} \psi_g^+(\vec{r}, \hat{\Omega}) + \Sigma_{t,g}(\vec{r}) \psi_g^-(\vec{r}, \hat{\Omega}) = W_g^-(\vec{r}, \hat{\Omega}) + S_g^-(\vec{r}, \hat{\Omega}). \quad (7)$$

The new even- and odd-parity sources in Eqs. (6) and (7), along with the within group scattering kernels are defined as

$$S_g^\pm(\vec{r}, \hat{\Omega}) = \frac{1}{2} S_g(\vec{r}, \hat{\Omega}) \pm \frac{1}{2} S_g(\vec{r}, -\hat{\Omega}) \quad (8)$$

$$W_g^\pm(\vec{r}, \hat{\Omega}) = \int \Sigma_{s,g \rightarrow g}^\pm(\vec{r}, \hat{\Omega} \cdot \hat{\Omega}') \psi_g^\pm(\vec{r}, \hat{\Omega}') d\hat{\Omega}' = \int \sum_m \Sigma_{s,g \rightarrow g,m}^\pm(\vec{r}) P_m^\pm(\hat{\Omega} \cdot \hat{\Omega}') \psi_g^\pm(\vec{r}, \hat{\Omega}') d\hat{\Omega}' \quad (9)$$

Note that the scattering cross sections are assumed to be expanded in a set of Legendre polynomials.

For our studies we make use of the second-order even parity transport equation and therefore solve the odd parity transport equation, Eq. (7), for $\psi_g^-(\vec{r}, \hat{\Omega})$ and substitute it into Eq. (6) to obtain

$$\hat{\Omega} \cdot \vec{\nabla} \frac{-1}{\Sigma_{t,g}(\vec{r})} \left[\hat{\Omega} \cdot \vec{\nabla} \psi_g^+(\vec{r}, \hat{\Omega}) - W_g^-(\vec{r}, \hat{\Omega}) - S_g^-(\vec{r}, \hat{\Omega}) \right] + \Sigma_{t,g}(\vec{r}) \psi_g^+(\vec{r}, \hat{\Omega}) = W_g^+(\vec{r}, \hat{\Omega}) + S_g^+(\vec{r}, \hat{\Omega}) \quad (10)$$

The spherical harmonics approximation is relatively unique compared to the other methods of treating the angular variable in that the within group anisotropic scattering moments can be directly solved for, thereby eliminating within group scattering iterations. Since the spherical harmonics method is the primary focus of this work, the actual steps required to achieve this transformation are displayed.

First, the even and odd parity flux are expanded into orthonormal spherical harmonics such that we can write

$$\psi_g^+(\vec{r}, \Omega) = \sum_{l=0,2}^{\infty} \sum_{m=-l}^l Y_{l,m}(\hat{\Omega}) \psi_{g,l,m}^+(\vec{r}) = \mathbf{Y}_+^T(\hat{\Omega}) \boldsymbol{\psi}_g^+(\vec{r}) \quad (11)$$

$$\psi_g^-(\vec{r}, \Omega) = \sum_{l=1,3}^{\infty} \sum_{m=-l}^l Y_{l,m}(\hat{\Omega}) \psi_{g,l,m}^-(\vec{r}) = \mathbf{Y}_-^T(\hat{\Omega}) \psi_g^-(\vec{r}) \quad (12)$$

where $\mathbf{Y}_{\pm}(\hat{\Omega})$ represent vectors of even- and odd-parity spherical harmonics. We can weight Eq. (7) with the an odd parity set of spherical harmonics and integrate over the angular domain to obtain the following expression

$$\int d\Omega \mathbf{Y}_-^T(\hat{\Omega}) \left[\hat{\Omega} \cdot \vec{\nabla} \mathbf{Y}_+^T(\hat{\Omega}) \psi_g^+(\vec{r}) + \Sigma_{t,g}(\vec{r}) \mathbf{Y}_-^T(\hat{\Omega}) \psi_g^-(\vec{r}) = W_g^-(\vec{r}, \hat{\Omega}) + S_g^-(\vec{r}, \hat{\Omega}) \right]. \quad (13)$$

Each term in Eq. (13) can be simplified as shown in Eqs. (14) through (17).

$$\int d\Omega \mathbf{Y}_-^T(\hat{\Omega}) \hat{\Omega} \cdot \vec{\nabla} \mathbf{Y}_+^T(\hat{\Omega}) \psi_g^+(\vec{r}) = \mathbf{V}^T \cdot \vec{\nabla} \psi_g^+(\vec{r}) \quad (14)$$

$$\int d\Omega \mathbf{Y}_-^T(\hat{\Omega}) \Sigma_{t,g}(\vec{r}) \mathbf{Y}_-^T(\hat{\Omega}) \psi_g^-(\vec{r}) = \Sigma_{t,g}(\vec{r}) \psi_g^-(\vec{r}) \quad (15)$$

$$\begin{aligned} \int d\Omega \mathbf{Y}_-^T(\hat{\Omega}) W_g^-(\vec{r}, \hat{\Omega}) &= \int d\Omega \mathbf{Y}_-^T(\hat{\Omega}) \sum_m \int \Sigma_{s,g \rightarrow g,m}^-(\vec{r}) P_m^-(\hat{\Omega} \cdot \hat{\Omega}') \psi_g^-(\vec{r}, \hat{\Omega}') d\hat{\Omega}' \\ &= \int d\Omega \mathbf{Y}_-^T(\hat{\Omega}) \int \mathbf{Y}_-^T(\hat{\Omega}) \Sigma_{s,g \rightarrow g}^-(\vec{r}) \mathbf{Y}_-(\hat{\Omega}') \psi_g^-(\vec{r}, \hat{\Omega}') d\hat{\Omega}' \\ &= \Sigma_{s,g \rightarrow g}^-(\vec{r}) \psi_g^-(\vec{r}) \end{aligned} \quad (16)$$

$$\int d\Omega \mathbf{Y}_-^T(\hat{\Omega}) S_g^-(\vec{r}, \hat{\Omega}) = \int d\Omega \mathbf{Y}_-^T(\hat{\Omega}) \mathbf{Y}_-^T(\hat{\Omega}) \mathbf{S}_g^-(\vec{r}) = \mathbf{S}_g^-(\vec{r}) \quad (17)$$

$\Sigma_{s,g \rightarrow g}^-(\vec{r})$ is an angular identity like matrix with the diagonal elements corresponding to the Legendre moments of the scattering kernel (properly aligned with the set of spherical harmonics). Combining these expressions with Eq. (13) yields Eq. (18).

$$\mathbf{V}^T \cdot \vec{\nabla} \psi_g^+(\vec{r}) + \Sigma_{t,g}(\vec{r}) \psi_g^-(\vec{r}) = \Sigma_{s,g \rightarrow g}^-(\vec{r}) \psi_g^-(\vec{r}) + \mathbf{S}_g^-(\vec{r}) \quad (18)$$

Equation (18) is now solved for the odd parity flux as shown in Eq. (19).

$$\psi_g^-(\vec{r}) = -\tilde{\Sigma}_{s,g}^-(\vec{r}) \mathbf{V}^T \cdot \vec{\nabla} \psi_g^+(\vec{r}) + \tilde{\Sigma}_{s,g}^-(\vec{r}) \mathbf{S}_g^-(\vec{r}) \quad (19)$$

where the components of the new cross section vector $\tilde{\Sigma}_{s,g}^-(\vec{r})$ are defined as

$$\tilde{\Sigma}_{s,g,m}^-(\vec{r}) = \frac{1}{\Sigma_{t,g}(\vec{r}) - \Sigma_{s,g \rightarrow g,m}^-(\vec{r})} \quad (20)$$

We can multiply Eq. (19) by the set of odd parity functions to obtain

$$\psi_g^-(\vec{r}, \hat{\Omega}) = \mathbf{Y}_-^T(\hat{\Omega}) \psi_g^-(\vec{r}) = -\mathbf{Y}_-^T(\hat{\Omega}) \tilde{\Sigma}_{s,g}^-(\vec{r}) \mathbf{V}^T \cdot \vec{\nabla} \psi_g^+(\vec{r}) + \mathbf{Y}_-^T(\hat{\Omega}) \tilde{\Sigma}_{s,g}^-(\vec{r}) \mathbf{S}_g^-(\vec{r}) \quad (21)$$

We can now substitute this form into Eq. (6) to obtain the second-order even-parity form of the transport equation.

2.2. Weak Form of the Even Parity Equation

To solve for the even-parity flux, we weight Eq. (6) with a set of even-parity functions $\lambda^+(\vec{r}, \hat{\Omega})$ and integrate over space and angle. This gives the weak form of the even-parity transport equation

$$\int dV \int d\Omega \lambda^+(\vec{r}, \hat{\Omega}) \left[\hat{\Omega} \cdot \vec{\nabla} \psi_g^-(\vec{r}, \hat{\Omega}) + \Sigma_{t,g}(\vec{r}) \psi_g^+(\vec{r}, \hat{\Omega}) = W_g^+(\vec{r}, \hat{\Omega}) + S_g^+(\vec{r}, \hat{\Omega}) \right], \quad (22)$$

where the integration is over the volume of the domain. Applying the divergence theorem, we can modify the derivative of the odd-parity flux to obtain

$$\begin{aligned}
 & \int \int \left[-\hat{\Omega} \cdot \bar{\nabla} \lambda^+(\bar{r}, \hat{\Omega}) \psi_g^-(\bar{r}, \hat{\Omega}) + \lambda^+(\bar{r}, \hat{\Omega}) \Sigma_{t,g}(\bar{r}) \psi_g^+(\bar{r}, \hat{\Omega}) \right] d\Omega dV \\
 &= \int \int \left[\lambda^+(\bar{r}, \hat{\Omega}) W_g^+(\bar{r}, \hat{\Omega}) + \lambda^+(\bar{r}, \hat{\Omega}) S_g^+(\bar{r}, \hat{\Omega}) \right] d\Omega dV \\
 & - \oint \int \hat{\Omega} \cdot \hat{n} \lambda^+(\bar{r}, \hat{\Omega}) \psi_g^-(\bar{r}, \hat{\Omega}) d\Omega d\Gamma
 \end{aligned} \tag{23}$$

where \hat{n} is the outward normal from the domain surface, Γ .

The incoming angular flux, $\psi_\Gamma(\bar{r}, \hat{\Omega})$, is known on the domain surface and can be expressed for each group as

$$\psi_\Gamma(\bar{r}, \hat{\Omega}) = \psi_\Gamma^+(\bar{r}, \hat{\Omega}) + \psi_\Gamma^-(\bar{r}, \hat{\Omega}) \quad \bar{r} \in \Gamma, \hat{\Omega} \cdot \hat{n} < 0 \tag{24}$$

Modified natural boundary conditions can be obtained by forming the weighted residuals

$$\oint d\Gamma \int_{\hat{\Omega} \cdot \hat{n} < 0} d\Omega \lambda^+(\bar{r}, \hat{\Omega}) \left(\psi_\Gamma^+(\bar{r}, \hat{\Omega}) + \psi_\Gamma^-(\bar{r}, \hat{\Omega}) - \psi_\Gamma(\bar{r}, \hat{\Omega}) \right) = 0 \tag{25}$$

Using angular parity arguments, we can take the boundary term from Eq. (23) and write

$$\begin{aligned}
 & \oint d\Gamma \int d\Omega \hat{\Omega} \cdot \hat{n} \lambda^+(\bar{r}, \hat{\Omega}) \psi_\Gamma^-(\bar{r}, \hat{\Omega}) = \\
 & \oint d\Gamma \int d\Omega |\hat{\Omega} \cdot \hat{n}| \lambda^+(\bar{r}, \hat{\Omega}) \psi_\Gamma^+(\bar{r}, \hat{\Omega}) + 2 \oint d\Gamma \int_{\hat{\Omega} \cdot \hat{n} < 0} d\Omega \hat{\Omega} \cdot \hat{n} \lambda^+(\bar{r}, \hat{\Omega}) \psi_\Gamma(\bar{r}, \hat{\Omega})
 \end{aligned} \tag{26}$$

Substitution of Eq. (26) into Eq. (23) yields the primal form of the second-order equation with modified natural boundary conditions

$$\begin{aligned}
 & \int \int \left[-\hat{\Omega} \cdot \bar{\nabla} \lambda^+(\bar{r}, \hat{\Omega}) \psi_g^-(\bar{r}, \hat{\Omega}) + \lambda^+(\bar{r}, \hat{\Omega}) \Sigma_{t,g}(\bar{r}) \psi_g^+(\bar{r}, \hat{\Omega}) \right] d\Omega dV \\
 &= \int \int \left[\lambda^+(\bar{r}, \hat{\Omega}) W_g^+(\bar{r}, \hat{\Omega}) + \lambda^+(\bar{r}, \hat{\Omega}) S_g^+(\bar{r}, \hat{\Omega}) \right] d\Omega dV \\
 & - \oint d\Gamma \int d\Omega |\hat{\Omega} \cdot \hat{n}| \lambda^+(\bar{r}, \hat{\Omega}) \psi_g^+(\bar{r}, \hat{\Omega}) - 2 \oint d\Gamma \int_{\hat{\Omega} \cdot \hat{n} < 0} d\Omega \hat{\Omega} \cdot \hat{n} \lambda^+(\bar{r}, \hat{\Omega}) \psi_\Gamma(\bar{r}, \hat{\Omega})
 \end{aligned} \tag{27}$$

Equations (21), (23), and (27) form the basic pieces of the second-order even parity formulation we want to implement. We therefore introduce a functional notation for the unknown quantities of Eq. (23)

$$\begin{aligned}
 T \left[\psi_g^+(\bar{r}, \hat{\Omega}), \psi_g^-(\bar{r}, \hat{\Omega}) \right] &= \int \int \left[-\hat{\Omega} \cdot \bar{\nabla} \lambda^+(\bar{r}, \hat{\Omega}) \psi_g^-(\bar{r}, \hat{\Omega}) + \lambda^+(\bar{r}, \hat{\Omega}) \Sigma_{t,g}(\bar{r}) \psi_g^+(\bar{r}, \hat{\Omega}) \right] d\Omega dV \\
 & - \int \int \left[\lambda^+(\bar{r}, \hat{\Omega}) W_g^+(\bar{r}, \hat{\Omega}) + \lambda^+(\bar{r}, \hat{\Omega}) S_g^+(\bar{r}, \hat{\Omega}) \right] d\Omega dV \\
 & + \oint \int \hat{\Omega} \cdot \hat{n} \lambda^+(\bar{r}, \hat{\Omega}) \psi_g^-(\bar{r}, \hat{\Omega}) d\Omega d\Gamma
 \end{aligned} \tag{28}$$

By inspection, we know that further substitution of Eq. (26) into Eq. (28) would yield a similar functional where the unknown odd parity boundary flux is replaced by the component of the known incoming angular flux. Similarly, substitution of Eq. (21) will yield a functional whose only unknown is the internal even parity angular flux.

2.3. Finite Element Implementation

We continue by investigating the spatial approximation, designated as the finite element method. In the finite element method, the problem domain is subdivided using a finite element mesh as seen in Figure 1 where the global summation of Eq. (29) is defined in terms of the element contributions given by Eq. (30).

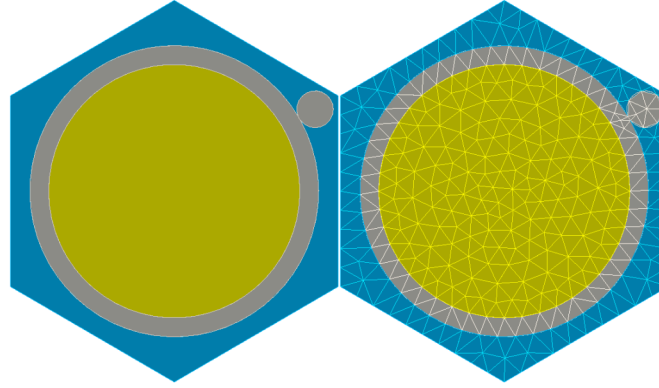


Figure 1. Imposition of a Triangular Finite Element Mesh for a Fast Reactor Fuel Pin

$$T[\psi_g^+(\vec{r}, \hat{\Omega}), \psi_g^-(\vec{r}, \hat{\Omega})] = \sum_{e=1}^{elements} T_e[\psi_{g,e}^+(\vec{r}, \hat{\Omega}), \psi_{g,e}^-(\vec{r}, \hat{\Omega})]. \quad (29)$$

$$\begin{aligned} T_e[\psi_{g,e}^+(\vec{r}, \hat{\Omega}), \psi_{g,e}^-(\vec{r}, \hat{\Omega})] = & \int \int [-\hat{\Omega} \cdot \vec{\nabla} \lambda_e^+(\vec{r}, \hat{\Omega}) \psi_{g,e}^-(\vec{r}, \hat{\Omega}) + \lambda_e^+(\vec{r}, \hat{\Omega}) \Sigma_{t,g}^e(\vec{r}) \psi_{g,e}^+(\vec{r}, \hat{\Omega})] d\Omega dV \\ & - \int \int [\lambda_e^+(\vec{r}, \hat{\Omega}) W_{g,e}^+(\vec{r}, \hat{\Omega}) + \lambda_e^+(\vec{r}, \hat{\Omega}) S_{g,e}^+(\vec{r}, \hat{\Omega})] d\Omega dV \\ & + \oint \hat{\Omega} \cdot \hat{n} \lambda_e^+(\vec{r}, \hat{\Omega}) \psi_{g,e}^-(\vec{r}, \hat{\Omega}) d\Omega d\Gamma \end{aligned} \quad (30)$$

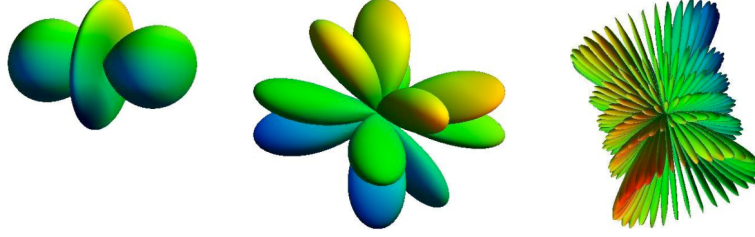
Each finite element in the mesh is defined through the use of spatial vertex points (typically called nodes in the finite element literature) and the cross sections within each element are assumed to be spatially flat.³ The imposition of a continuous finite element approximation to the even parity angular flux and the even parity weighting function eliminates the general boundary term from the system of equations for adjoining elements. As a consequence, the surface term in Eq. (30) only exists for those elements that lie along the outer problem boundary.

2.4. Combined Space-Angle Approximations

The definition of the spherical harmonic functions,² examples of which are shown in Figure 2, are not included here for brevity. The focus for this work is on the use of the sine and cosine series defined as

$$\begin{aligned} Y_{\ell,m}^e(\hat{\Omega}) &= \sqrt{C_\ell^m} \cdot P_\ell^m(\mu) \cdot \cos(m\phi) \\ Y_{\ell,m}^o(\hat{\Omega}) &= \sqrt{C_\ell^m} \cdot P_\ell^m(\mu) \cdot \sin(m\phi) \end{aligned} \quad C_\ell^m = \frac{(2\ell+1)(\ell-m)!}{(\ell+m)!}. \quad (31)$$

What is unique about Eq. (31) is that the functions $Y_{\ell,m}^e(\hat{\Omega})$ are even parity with respect to ϕ and the functions $Y_{\ell,m}^o(\hat{\Omega})$ are odd parity with respect to ϕ . Focusing only on the angular variable, the even parity flux $\psi_g^+(\vec{r}, \hat{\Omega})$, weight function $\lambda_+(\vec{r}, \hat{\Omega})$, and odd parity flux can be approximated with this set of angular functions in a vector form given by


Figure 2. Some Example Spherical Harmonic Trial Functions

$$\psi_g^+(\vec{r}, \hat{\Omega}) = \sum_{l=0,2,\dots}^{N-1} \sum_{m=-l}^l Y_{\ell,m}^e(\hat{\Omega}) \psi_{l,m}^+(\vec{r}) = \mathbf{Y}_+^T(\hat{\Omega}) \boldsymbol{\psi}_g^+(\vec{r}) \quad (32)$$

$$\lambda_+(\vec{r}, \hat{\Omega}) = \sum_{l=0,2,\dots}^{N-1} \sum_{m=-l}^l Y_{\ell,m}^e(\hat{\Omega}) \lambda_+^{l,m}(\vec{r}) = \mathbf{Y}_+^T(\hat{\Omega}) \boldsymbol{\lambda}_+(\vec{r}) \quad (33)$$

$$\psi_g^-(\vec{r}, \hat{\Omega}) = \sum_{l=1,3,\dots}^N \sum_{m=-l}^l Y_{\ell,m}^o(\hat{\Omega}) \psi_{l,m}^-(\vec{r}) = \mathbf{Y}_-^T(\hat{\Omega}) \boldsymbol{\psi}_g^-(\vec{r}) \quad (34)$$

Equations (21), (27), (32), (33) and (34) can be substituted into Eq. (30) to obtain the following functional

$$\begin{aligned} \mathbf{T}_e[\boldsymbol{\psi}_g^+(\vec{r})] = & \int \int -\hat{\Omega} \cdot \vec{\nabla} \boldsymbol{\lambda}_+^T(\vec{r}) \mathbf{Y}_+(\hat{\Omega}) \mathbf{Y}_-^T(\hat{\Omega}) \tilde{\boldsymbol{\Sigma}}_{s,g}^-(\vec{r}) \mathbf{V}^T \cdot \vec{\nabla} \boldsymbol{\psi}_g^+(\vec{r}) d\Omega dV \\ & + \int \int \boldsymbol{\lambda}_+^T(\vec{r}) \mathbf{Y}_+(\hat{\Omega}) \boldsymbol{\Sigma}_{t,g}(\vec{r}) \mathbf{Y}_+(\hat{\Omega}) \boldsymbol{\psi}_g^+(\vec{r}) d\Omega dV \\ & - \int \int \boldsymbol{\lambda}_+^T(\vec{r}) \mathbf{Y}_+(\hat{\Omega}) \mathbf{W}_g^+(\vec{r}, \hat{\Omega}) d\Omega dV \\ & - \int \int \boldsymbol{\lambda}_+^T(\vec{r}) \mathbf{Y}_+(\hat{\Omega}) \mathbf{S}_g^+(\vec{r}, \hat{\Omega}) d\Omega dV \\ & - \int \int \hat{\Omega} \cdot \vec{\nabla} \boldsymbol{\lambda}_+^T(\vec{r}) \mathbf{Y}_+(\hat{\Omega}) \mathbf{Y}_-^T(\hat{\Omega}) \tilde{\boldsymbol{\Sigma}}_{s,g}^-(\vec{r}) \mathbf{S}_g^-(\vec{r}) d\Omega dV \\ & + \mathbf{BC}_g \end{aligned} \quad (35)$$

where the boundary condition term, which only exists for those elements along the problem domain boundary, is defined as:

$$\begin{aligned} \mathbf{BC}_g = & \oint \int \hat{\Omega} \cdot \hat{n} \boldsymbol{\lambda}_+^T(\vec{r}, \hat{\Omega}) \boldsymbol{\psi}_g^-(\vec{r}, \hat{\Omega}) d\Omega d\Gamma \\ = & -\oint d\Gamma \int d\Omega \left| \hat{\Omega} \cdot \hat{n} \right| \boldsymbol{\lambda}_+^T(\vec{r}) \mathbf{Y}_+(\hat{\Omega}) \mathbf{Y}_+(\hat{\Omega}) \boldsymbol{\lambda}_+(\vec{r}) - 2 \oint d\Gamma \int_{\hat{\Omega} \cdot \hat{n} < 0} d\Omega \hat{\Omega} \cdot \hat{n} \boldsymbol{\lambda}_+^T(\vec{r}) \mathbf{Y}_+(\hat{\Omega}) \boldsymbol{\psi}_g^-(\vec{r}, \hat{\Omega}) \end{aligned} \quad (36)$$

This system of equations can be compacted by defining the following angular matrices.

$$\mathbf{V}_K = \int \hat{\Omega} \mathbf{Y}_+(\hat{\Omega}) \mathbf{Y}_-^T(\hat{\Omega}) d\Omega \quad (37)$$

$$\mathbf{I}_{\pm} = \int \mathbf{Y}_{\pm}(\hat{\Omega}) \mathbf{Y}_{\pm}^T(\hat{\Omega}) d\Omega \quad (38)$$

Substituting these matrix definitions into Eq. (35) yields

$$\begin{aligned} \mathbf{T}_e[\boldsymbol{\psi}_g^+(\vec{r})] = & - \int \vec{\nabla} \boldsymbol{\lambda}_+^T(\vec{r}) \cdot \mathbf{V} \tilde{\boldsymbol{\Sigma}}_{s,g}^-(\vec{r}) \mathbf{V}^T \cdot \vec{\nabla} \boldsymbol{\psi}_g^+(\vec{r}) dV + \int \boldsymbol{\lambda}_+^T(\vec{r}) \boldsymbol{\Sigma}_{t,g}(\vec{r}) \mathbf{I}_+ \boldsymbol{\psi}_g^+(\vec{r}) dV \\ & - \int \boldsymbol{\lambda}_+^T(\vec{r}) \boldsymbol{\Sigma}_{s,g \rightarrow g}^+ \boldsymbol{\psi}_g^+(\vec{r}) dV - \int \boldsymbol{\lambda}_+^T(\vec{r}) \mathbf{I}_+ \mathbf{S}_g^+(\vec{r}) dV \\ & - \int \vec{\nabla} \boldsymbol{\lambda}_+^T(\vec{r}) \cdot \mathbf{V} \tilde{\boldsymbol{\Sigma}}_{s,g}^-(\vec{r}) \mathbf{S}_g^-(\vec{r}) dV + \mathbf{BC}_g \end{aligned} \quad (39)$$

The application of the finite element approximation to the flux, source, and weighting function representations results in

$$\boldsymbol{\psi}_g^\pm(\vec{r}, \hat{\Omega}) = \mathbf{Y}_\pm^T(\hat{\Omega}) \otimes \mathbf{L}_e^T(\vec{r}) \tilde{\boldsymbol{\psi}}_{g,e}^\pm \quad (40)$$

$$S_g^\pm(\vec{r}, \Omega) = \mathbf{Y}_\pm^T(\hat{\Omega}) \otimes \mathbf{L}_e^T(\vec{r}) \tilde{\boldsymbol{\psi}}_{g,e}^\pm \quad (41)$$

$$\lambda^+(\vec{r}, \hat{\Omega}) = \mathbf{Y}_+^T(\hat{\Omega}) \otimes \mathbf{L}_e^T(\vec{r}) \quad (42)$$

where \otimes represents a tensor product of the spatial and angular vector of trial functions. Substitution of Eqs. (40) through (42) into Eq. (39) for a given element yields the following spatial matrices

$$P_{e_{K,L}} = \int \bar{\mathbf{V}}_K L_e(\vec{r}) \bar{\mathbf{V}}_L^T L_e^T(\vec{r}) dV_e, \quad (43)$$

$$U_{e_K} = \int L_e(\vec{r}) \bar{\mathbf{V}}_K L_e^T(\vec{r}) dV_e, \quad (44)$$

and

$$F_e = \int L_e(\vec{r}) L_e(\vec{r}) dV_e. \quad (45)$$

Introducing these equations into Eq. (39) yields the following set of algebraic equations for each element

$$\begin{aligned} \mathbf{T}_e \left[\tilde{\boldsymbol{\psi}}_{g,e}^+ \right] = & - \sum_{K,L} \mathbf{V}_K \tilde{\boldsymbol{\Sigma}}_{s,g}^- \mathbf{V}_L^T \otimes P_{e_{K,L}} \tilde{\boldsymbol{\psi}}_{g,e}^+ + \sum_{t,g} \mathbf{I}_+ \otimes F_e \tilde{\boldsymbol{\psi}}_{g,e}^+ \\ & - \sum_{s,g \rightarrow g}^+ \otimes F_e \tilde{\boldsymbol{\psi}}_{g,e}^+ - \mathbf{I}_+ \otimes F_e \tilde{\boldsymbol{\Sigma}}_{g,e}^+ - \sum_K \mathbf{V}_K \tilde{\boldsymbol{\Sigma}}_{s,g}^- \otimes U_{e_K}^T \tilde{\boldsymbol{\Sigma}}_{g,e}^- + \mathbf{BC}_{g,e}. \end{aligned} \quad (46)$$

Equation 46 can further be simplified by defining the matrices and vectors

$$A_{g,e} = - \sum_{K,L} \mathbf{V}_K \tilde{\boldsymbol{\Sigma}}_{s,g}^- \mathbf{V}_L^T \otimes P_{e_{K,L}} + \sum_{t,g} \mathbf{I}_+ \otimes F_e - \sum_{s,g \rightarrow g}^+ \otimes F_e, \quad (47)$$

$$\tilde{\boldsymbol{s}}_{g,e}^+ = \mathbf{I}_+ \otimes F_e \tilde{\boldsymbol{\Sigma}}_{g,e}^+, \quad (48)$$

$$\tilde{\boldsymbol{s}}_{g,e}^- = \sum_K \mathbf{V}_K \tilde{\boldsymbol{\Sigma}}_{s,g}^- \otimes U_{e_K}^T \tilde{\boldsymbol{\Sigma}}_{g,e}^-, \quad (49)$$

to obtain

$$\mathbf{T}_e \left[\tilde{\boldsymbol{\psi}}_{g,e}^+ \right] = A_{g,e} \tilde{\boldsymbol{\psi}}_{g,e}^+ - \tilde{\boldsymbol{s}}_{g,e}^+ - \tilde{\boldsymbol{s}}_{g,e}^- + \mathbf{BC}_{g,e}. \quad (50)$$

3. BENCHMARK CALCULATIONS AND RESULTS

As mentioned, the preceding second-order formulation has been implemented using a spherical harmonics approximation of the angular variable. Clearly for a large spatial domain and high-order angular approximation, the matrix resulting from Eqs. (29) and (50) cannot be directly inverted due to the computational burden and storage expense. As a consequence, we have made use of the conjugate gradient solver available in the PETSc (Portable, Extensible Toolkit for Scientific Computation) package developed at ANL.⁵ PETSc provides a variety of linear and nonlinear solvers for partial differential equations (PDE) on high-performance parallel computing platforms. It provides many types of preconditioners that are commonly used to improve the convergence rate of linear iterative methods. So far we have experimented with incomplete Cholesky factorization (with various fill levels) and successive over relaxation preconditioners. At this stage, the existing set of PETSc preconditioners does not take full advantage of the structure of the matrix (especially when higher-order angular approximations

are implemented). We are therefore investigating some custom implementations for the preconditioners of interest in PETSc.

3.1. Takeda 4 Benchmark

The first benchmark solved is the fourth Takeda benchmark, the details of which can be found in reference 7. This benchmark is used to check the general solution capability of transport methods since it requires a relatively low angular approximation and contains virtually no heterogeneity. The geometrical 1/6 symmetry representation is given in Figure 3 along with the mesh that displayed full spatial convergence on the control rod withdrawn problem. The cross sections were provided and reference solutions were obtained using the VIM Monte Carlo code⁸ in multigroup mode. In this benchmark, three configurations were specified where the control rod is inserted fully, half, or removed. Figure 4 shows the four group flux solutions for the control rod half inserted problem. The VIM Monte Carlo solution for the full inserted control rod is 0.88001 ± 0.00038 , for the half inserted control rod is 0.9834 ± 0.00039 , and for the withdrawn control rod is 1.09515 ± 0.00040 .

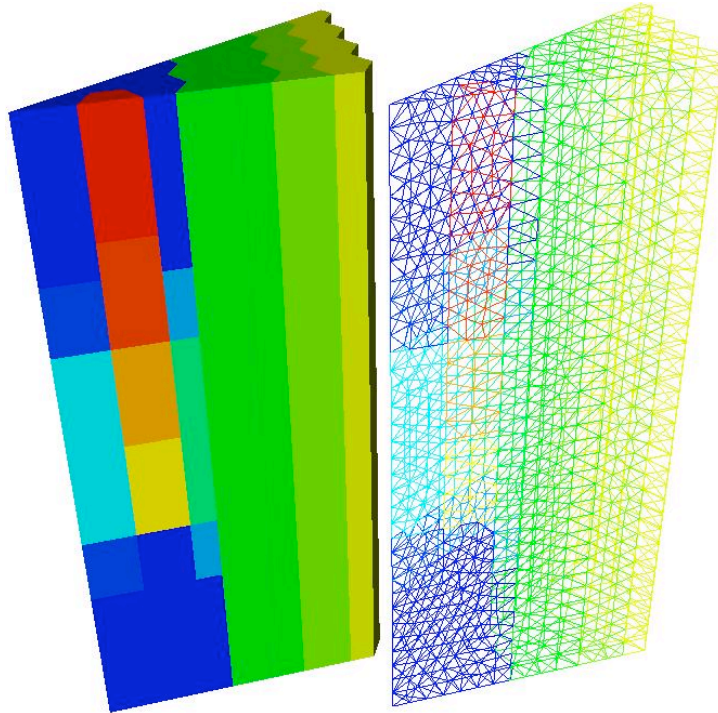


Figure 3. Fourth Takeda Benchmark Geometry and Mesh

The relatively large inaccuracy in these results limits the accuracy verification of the new code and thus additional, comparative solutions were obtained using the nodal spherical harmonics code VARIANT. Table I gives the solutions obtained using the VARIANT code and the P_NFE component of UNIC. All of these calculations were completed on the Jazz cluster at Argonne using 16 to 64 processors. From our space-angle convergence analysis, we believe the solutions obtained with P_NFE and VARIANT codes are good although additional spatial refinement might be necessary in both codes to get agreement. There is also some residual error in the Monte Carlo solutions likely due to insufficient fission source convergence. The P₇ flux solution obtained

using the P_NFE solution on the half inserted control rod configuration is given at the bottom of Figure 4 (first through fourth energy group fluxes are given left to right).

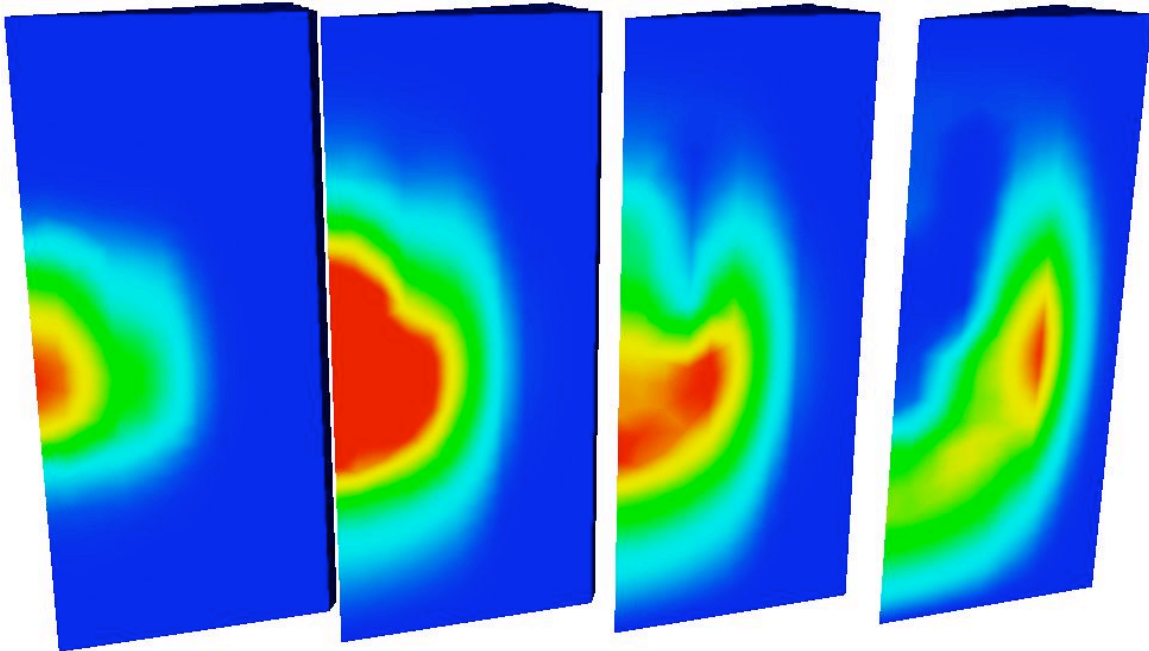


Figure 4. Fourth Takeda Benchmark Half Inserted Flux Results

Table I. Eigenvalue Solutions for the Takeda #4 Benchmark

Angular Order	Fully Inserted		Half Inserted		Withdrawn	
	PNFE	VARIANT	PNFE	VARIANT	PNFE	VARIANT
1	0.85161	0.85423	0.95757	0.96063	1.07335	1.07543
3	0.87554	0.87749	0.98010	0.98195	1.09305	1.09441
5	0.87761	0.87949	0.98188	0.98364	1.09444	1.09577
7	0.87800	0.87992	0.98229	0.98405	1.09481	1.09614
9	0.87811	0.88003	0.98241	0.98404	1.09493	1.09628
11	0.87814	0.88009	0.98245	0.98415	1.09498	1.09636
	Error (pcm)		Error (pcm)		Error (pcm)	
1	-2840	-2578	-2583	-2277	-2180	-1972
3	-447	-252	-330	-145	-210	-74
5	-240	-52	-152	24	-71	62
7	-201	-9	-111	65	-34	99
9	-190	2	-99	64	-22	113
11	-187	8	-95	75	-17	121

3.2. ABTR Single Pin Benchmark

A more difficult benchmark derived from the advanced burner test reactor (ABTR) design currently being studied¹⁰ was chosen as the other benchmark. Figure 5 describes the geometrical layout of the benchmark geometry; more specific detail on the ABTR, specifically the

compositions, can be found in reference 10. Reflected boundary conditions are assumed in the radial plane and vacuum boundary conditions are assumed at the upper and lower boundaries. Note that a companion paper presents a more complicated geometrical layout used for analysis of a thermal hydraulic coupling simulation. The purpose of this benchmark was to investigate the impact of homogenization on the fast reactor system and to determine what level of geometrical representation is necessary for an assembly and thus the full core problem. A five energy group structure was implemented for this study. Cross sections were generated at nominal fuel temperatures using the MC²-2 cross section generation code.¹¹ The model utilized also reduced the axial domain of interest in Figure 5 from 3.4568 m to 1.2698 m about the center of the active core such that the unimportant neutronic portions of the domain are eliminated for this study. The wire wrap is also smeared into the coolant region (~3% of the total volume) for simplicity in the benchmark.

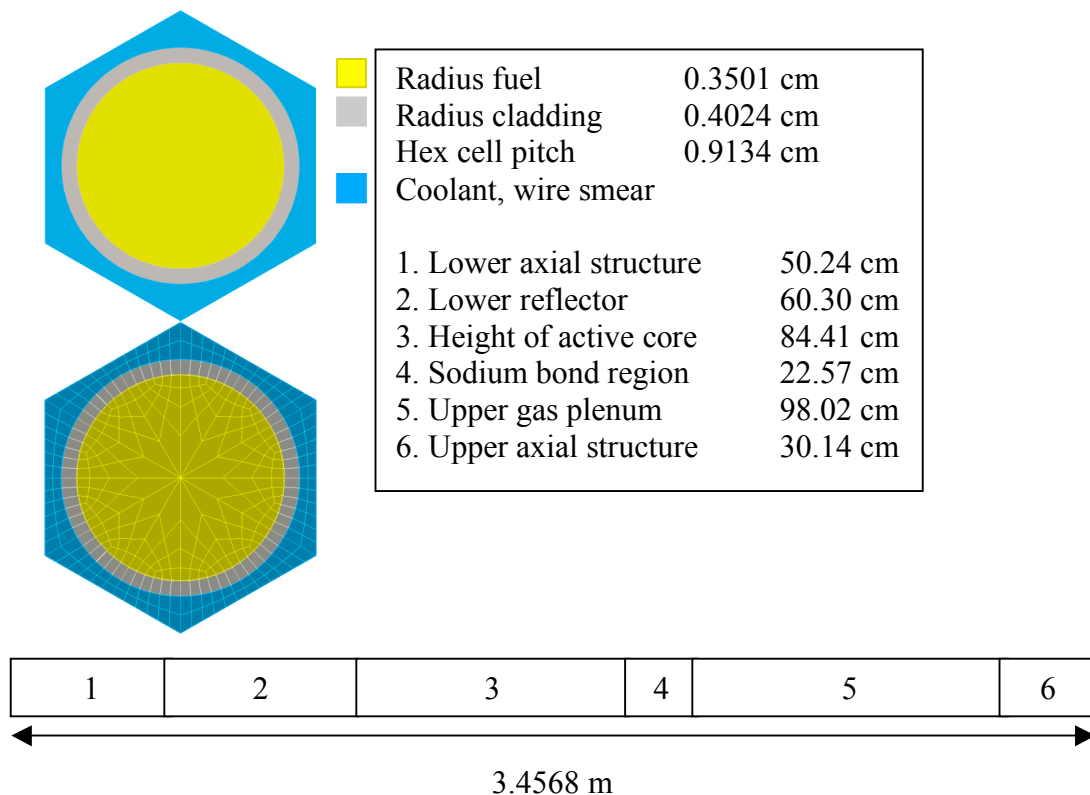


Figure 5. ABTR Single Pin Geometry and Radial Finite Element Mesh

The reference solution was obtained with the Monte Carlo code MCNP¹² in multigroup mode using the set of multigroup cross sections derived from MC²-2. With the above stated modifications to the geometry, MCNP reported an eigenvalue of 1.57268 ± 0.00008 for the heterogeneous calculation. Table II shows the solutions using the P_NFE code using the explicit geometry of Figure 5 and two radial homogenization schemes. A very fine spatial mesh was chosen for all three problems and the comparative results of a coarser mesh are given for the explicit geometry and first homogenization scheme (mesh not shown for brevity). In the first homogenization scheme, the cladding and coolant compositions were homogenized together without flux weighting. The other homogenization scheme smears all radial regions together effectively defining a one-dimensional geometry. All of these calculations were completed on

the Jazz cluster at Argonne using between 16 and 128 processors. As can be seen, only a narrow range of angular approximations were attempted with a significant amount of error still present. Our ongoing work has indicated that additional angular refinement is necessary in the heterogeneous calculations to match the Monte Carlo solution due to the presence of discontinuities in the angular flux at the interface of the fuel cylinder.

Table II. Eigenvalues for the ABTR Benchmark Problem.

P_N	Explicit Geometry		Homogenized Cladding+Coolant		Completely Homogenized
	Coarse	Fine	Coarse	Fine	Fine
1	1.51661	1.51696	1.54600	1.54633	1.56795
3	1.54068	1.54127	1.55738	1.55780	1.57004
5	1.54953	1.55067	1.56097	1.56147	1.57009
7	1.55408	1.55556	1.56287	1.56346	1.57011
9	1.55675	1.55852	1.56401	1.56468	1.57012
11	1.55844		1.56474		1.57013

4. CONCLUSIONS

The development of a second-order solver based on the spherical harmonics method called P_N FE was introduced and the results of two benchmarks were shown. In general the results obtained for these benchmarks were very good within the obvious limitations of the method. The P_N FE component of the UNIC code is still in the testing and development phase and thus the problems are somewhat limited in size due to serial implementations. At present, we have not fully optimized the parallel execution of the method using the PETSc toolkit and thus additional work will include both results and detailed timing studies. With time we will migrate from these small scale calculations to large scale reactor simulations with thousands of processors. Our short term goal is to model the advanced burner test reactor with ~ 100 energy groups using a pin-cell homogenized geometry model. We estimate that this reactor problem will require ~ 10 million spatial degrees of freedom and a P_9 angular approximation.

Although it is unlikely that the spherical harmonics code can be relied upon for the explicit geometry calculations (discontinuities in the angular flux), there is still a need for a robust solver of homogeneous problems, such as the Takeda benchmark, due to the limitations of modern computational abilities. Also, this new code provides a path to move from the legacy neutronics codes currently used for reactor analysis based upon homogenous assembly calculations to a new set of tools under development in the UNIC framework where such coarse homogenization can be avoided if not eliminated entirely. With this capability, the uncertainty associated with modeling different reactors along with the use of exotic fuel forms currently proposed can be analyzed with greater confidence. Note that this work is complementary to the ongoing development of a three-dimensional method of characteristics code also being carried out in the UNIC framework.¹ Finally, the additional development of a second-order discrete ordinates or discontinuous angular finite element capability can widen the scope of neutron transport problems that can be solved using a second-order method.

ACKNOWLEDGMENTS

Argonne National Laboratory's work was supported by the U.S. Department of Energy, Office of Nuclear Energy, under contract DE-AC02-06CH11357. We gratefully acknowledge use of the "Jazz cluster" operated by the Laboratory Computing Resource Center at Argonne National Laboratory.

REFERENCES

1. G. Palmiotti, et al., "UNIC: Ultimate Neutronic Investigation Code", A companion paper in Joint International Topical Meeting on Mathematics and Computation, Supercomputing in Nuclear Applications, Apr. 15-19, Monterey, California, USA, 2007.
2. Lewis, E.E., and Miller Jr., W.F., Computational Methods of Neutron Transport. New York: John Wiley & Sons, 1984.
3. Reddy, J.N., An Introduction to the Finite Element Method, Second Edition. Boston, Massachusetts, McGraw-Hill, 1993.
4. G. Palmiotti, et al., "Status Report on High Fidelity Reactor Simulation," ANL-AFCI-175, 2006.
5. S. Balay, K. R. Buschelman, W. D. Gropp, D. K. Kaushik, M. G. Knepley, L. C. McInnes, and B. F. Smith. PETSc home page, (2002). <http://www.mcs.anl.gov/petsc>.
6. Amy Henderson, editor "Paraview Guide," Kitware, Inc. Authors: Squillacote. ISBN 1-930934-17-3.
7. T. Takeda and H. Ikeda, "3-D Neutron Transport Benchmarks," NEACRP-1-300 OECD/NEA, Organization of Economic Cooperation and Development/Nuclear Energy Agency March 1991.
8. Blomquist, R.N., "VIM- A Continuous Energy Neutronics and Photon Transport Code," Int. Topl. Mtg. Adv. In Mathematics, Computations and Reactor Physics, April 28-May 2, 1992, Pittsburgh, PA.
9. G. Palmiotti, E. E. Lewis & C. B. Carrico, "VARIANT: VARIational Anisotropic Nodal Transport for Multidimensional Cartesian and Hexagonal Geometry Calculation," Argonne National Laboratory ANL-95/40 1995.
10. Y. I. Chang, P. J. Finck, and C. Grandy, "Advanced Burner Test Reactor Preconceptual Design Report," ANL-ABR-1, ANL-AFCI-173, Sept (2006).
11. H. Henryson, II, B. J. Toppel, C. G. Stenberg, "MC²-2: A Code to Calculate Fast Neutron Spectra and Multigroup Cross Sections," ANL-8144, June 1976.
12. Judith F. Briesmeister and XTM. MCNPTM-A General Monte Carlo N-Particle Transport Code. LOS ALAMOS National Laboratory LA-12625-M, March 1997.